Journal of Superconductivity: Incorporating Novel Magnetism (© 2006)
DOI: 10.1007/s10948-005-0099-6

From Local Moment EPR in Superconductors to Nanoscale Ferromagnets

Klaus Baberschke[1]

Received 29 September 2004; accepted xxxx

Electron paramagnetic resonance (EPR) in metals has contributed a lot to the understanding of the electronic structure and magnetic properties in dilute alloys as well as in concentrated ferromagnets. We recall some pioneering work of the Kazan group and others, studying local moment EPR in superconductors. An SNS Josephson junction has been used as a microwave generator and as an EPR detector at once. EPR was also used to study the Kondo effect in the EPR g-shift and linewidth. Moreover, the high sensitivity of EPR (down to 10^{10} spins) allows to study single atomic layers of ferromagnets below and above the Curie temperature T_C as well as the spin fluctuations at T_C. The *in situ* ferromagnetic resonance (FMR) in ultrahigh vacuum (UHV) offers a unique possibility to study the interlayer exchange coupling (IEC) and spin dynamics of coupled ferromagnetic films. Furthermore, the magnetic resonance enables us to measure basic parameters of nanoscale magnets in absolute energy units (i.e., μeV/spin). The current status of the UHV-FMR in nanoscale ferromagnets will be discussed.

KEY WORDS: paramagnetic resonance; superconductors; ferromagnetic films.

1. INTRODUCTION

Since the discovery of the electron paramagnetic resonance by E. K. Zavoisky [1] in 1944 EPR has been used in a vast variety of applications and fundamental research. Not only in solid state physics but also for application in chemistry, biology, physics of liquids, etc. Photosynthetic reaction centers have been investigated, molecular motion in liquids was studied as well as photo-excited triplet states in molecules and many other areas. The broad scope of EPR in theory and experiment is also documented by the large number of distinguished award holders of the Zavoisky Award [2]. It is our impression that the main activity of modern development of the EPR focuses on $S = 1/2$ and triplet states dealing with s- and p-electron eigenstates. On the other hand, already at the XIVth Colloque Ampère in 1966 S. A. Al'tshuler pointed out that the EPR was of major importance for the development in the field of spin-lattice paramagnetic relaxation [3]. Here we are mostly dealing with 3d and 4f ions having a large degeneracy of $S = 5/2$ or even $J = 15/2$. Worldwide, several groups worked on the further development and application of the EPR in experiment and theory. We name only two: the Kazan group (S. A. Al'tshuler, B. I. Kochelaev, I. A. Garifullin) and the Oxford group (B. Bleaney and coworkers, an award holder of the Zavoisky Award, too) [4]. In the following some examples are given of EPR with paramagnetic 3d and 4f ions acting as pair breaking impurities in superconductors or as Kondo ions. Already one decade after the discovery of the EPR the same technique was used to study the ferromagnetic resonance (FMR). One of the pioneering groups in this field was the Berkeley group (Ch. Kittel and coworkers) [5]. Nowadays the FMR gained great attention to study magnetic nanostructures and quantum dots, important for the storage media technology as well as for fundamental aspects. In contrast to other experimental tools like Faraday- and Kerr-effect or spin-polarized photoemission which allow only to

[1]Institut für Experimentalphysik, Freie Universität Berlin, Arnimallee 14, D-14195, Berlin-Dahlem, Germany; email: bab@physik.fu-berlin.de.

study the ferromagnetic ground state (with a finite magnetization M), the magnetic resonance allows to study the concentrated magnet above and below T_C. This will be discussed in Section 4 and 5.

2. LOCAL MOMENT EPR IN SUPERCONDUCTORS

2.1 Pair Breaking Parameter

In 1966 at the XIVth Colloque Ampère magnetic resonance in superconductors was already discussed—but only nuclear resonance. The pioneering work of EPR in superconductors was published only in 1972 by the Kazan group [6]. The authors doped the type-II superconductor La_3In with 1% Gd and recorded an EPR signal close to $g \approx 2$. On the other hand already in 1960, A. A. Abrikosov and L. P. Gor'kov developed the theory that paramagnetic impurities act as scattering centers for Cooper pairs and consequently reduce the superconducting transition temperature T_C as a function of the concentration [7]. In other words, the spin-flip scattering of paramagnetic impurities in superconductors should not only be detectable in transport experiments measuring T_C as a function of the impurity concentration but should also be visible in the linewidth of an EPR signal. This question was addressed independently at the same time by three groups and published in 1973: the Kazan group investigated the Γ_7 ground state of Er in La. This was quite interesting because of the low external field needed for the Γ_7 resonance [8], the Orbach group detected Gd in $LaRu_2$ [9] and the Berlin group Gd in $CeRu_2$ [10]. The scattering mechanism is indicated in Fig. 1. There exist two magnetic subsystems, the paramagnetic impurities S and the conduction electrons σ. They are coupled via the exchange interaction $JS \cdot \sigma$. Both subsystems can scatter to the thermal bath via δ_{iL} and δ_{eL}. More important is however the spin-flip scattering between the two boxes. The scattering from the local impurity to the conduction electrons is given via the well-known Korringa equation

$$\hbar\delta_{ie} = \pi N^2(E_F)\langle J^2(k,k')\rangle kT. \qquad (1)$$

The scattering of the conduction electron at the localized magnetic impurity is also proportional to J^2 but multiplied by the number of unoccupied final states given by the multiplicity and the concentration

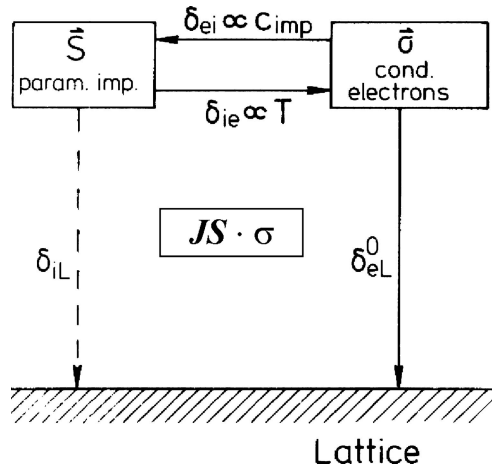

Fig. 1. Schematic relaxation paths between localized Spin S, conduction electron σ, and the thermal bath, see Eqs. (1) and (2).

$2S(S+1) \cdot c_{imp}$:

$$\hbar\delta_{ei} = \pi N(E_F)\langle J^2(k,k')\rangle 2S(S+1) \cdot c_{imp},$$

$$\left|\frac{dT_C}{dc_{imp}}\right| = \frac{3\hbar\pi}{16k_B}\frac{d\delta_{ei}}{dc_{imp}}. \qquad (2)$$

We are now in a position to measure the same observable, i.e., the pair-breaking parameter, in two independent experiments: (i) from the reduction of T_C in a static resistivity or susceptibility measurement and (ii) the EPR enables us to determine the same observable from a dynamic resonance experiment deduced from the linewidth analysis. Some typical results are given in Table I. Both experiments are in reasonably good agreement. This in turn confirms the Abrikosov-Gor'kov model of the pair breaking of Cooper pairs at paramagnetic impurities.

2.1 ac-Josephson Junction as EPR Spectrometer

Another interesting application is to use an ac-Josephson SNS-junction as an EPR spectrometer. If one applies a dc voltage across an SNS tunnel barrier a time-dependent shift of the phase for the

Table 1. Pair breaking parameter determined from T_C measurements and from EPR relaxation rates

Gd in		$LaOs_2$	$LaAl_2$	La (fcc)
$\left.\frac{dT_c}{dc}\right\|_{ESR}$	K/%	0.20	4.0	4.0
$\left.\frac{dT_c}{dc}\right\|_{exp}$	K/%	0.16	4.1	4.1

superconducting wave function is created according to

$$\partial(\theta_2 - \theta_1)/\partial t = -2\,\mathrm{eV}/\hbar, \quad \hbar\omega = 2\,\mathrm{eV},$$
$$483.6\,\mathrm{MHz} \mathrel{\hat{=}} 1\,\mu\mathrm{V}. \qquad (3)$$

In other words, we are able to use the Josephson junction as a microwave generator, i.e., 10 μV create a microwave of approximately 4.8 GHz. If we use a Pb/Au/Pb junction as the tunnel barrier and dope the normal conducting Au barrier with a small amount of Gd one should be able to detect the energy dissipation of the microwave in the *I–V* curve. Figure 2a shows schematically the crystal field splitting of Gd in Au. It splits in two doublets and one quartet. The doublet-quartet transitions are dipole-allowed, the doublet-doublet transition is dipole-forbidden. We expect therefore two resonance peaks in the ratio 12:20 and a missing resonance at the sum frequency of 32 relative units. The result is indicated in Fig. 2b. In the lower part the tunnel current as a function of the microwave frequency ν is shown. The two arrows indicate small dips which can be better visualized in the derivatives dI/dV unambiguously showing the two resonances and the missing peak at the Γ_6–Γ_7 position [11]. In other words, the Pb/Au/Pb tunnel barrier doped with Gd impurities acts as an EPR microwave generator and -detector at the same time. The energy dissipation of the microwaves given for discrete, excited eigenstates of the magnetic impurity is detected in the tunneling current as a function of the frequency/voltage. Both examples, the pair breaking of superconductivity by paramagnetic impurities and the creation of microwaves by the ac-Josephson effect seem to be a possible scenario for today's high-T_C-superconductor research.

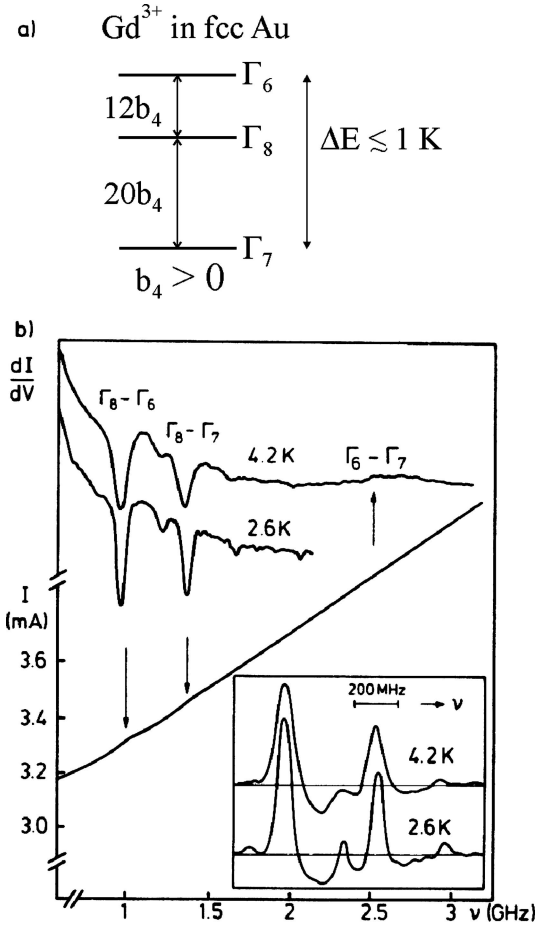

Fig. 2. Schematic crystal field splitting of the $S = 7/2$ manifold in cubic Au. dc-Josephson tunnel current I and its derivative dI/dV for a Pb/Au(Gd)/Pb barrier as a function of the ac-Josephson voltage which is transformed into frequency ν, see Eq. (3).

3. KONDO EFFECT IN THE EPR OF DILUTE ALLOYS

The exchange coupling between localized moments S and the conduction electron band σ is usually parameterized by the constant J as shown in Fig. 1. As discussed in the previous section this parameter enters twice into an EPR experiment: to the first power of J^1 as a positive or negative g-shift depending on a parallel or antiparallel coupling between localized moments and the conduction band, and to the second power J^2 in the (Korringa-) relaxation rate. If multi-particle effects like the screening of the localized spin by a "cloud of conduction electrons" with antiparallel spin alignment—the so-called Kondo effect—becomes important, the constant exchange coupling is renormalized by a logarithmic temperature dependence with a scaling parameter T_K. Below T_K the paramagnetic moment is mostly (or totally) screened by the conduction electrons and the paramagnetic properties vanish in susceptibility, specific heat, and other observables.

$$g - \text{shift} \propto J : \Delta g = \alpha d |\ln(T_K/T)|^{-1},$$
$$\text{linewidth} \propto J^2 : \delta_{ie}/\pi kT = \alpha^2 d |\ln(T_K/T)|^{-2}. \qquad (5)$$

If so, then also EPR should be able to see the logarithmic temperature dependence of the g-shift and the Korringa rate in the dilute Kondo alloy. An ideal system seems to be Au:Yb with T_K in the range of Millikelvin. The popular Kondo systems with 3d impurities usually have larger T_K's and

consequently a much broader EPR linewidth. On the other hand the low T_K produces an experimental difficulty, namely, an EPR spectrometer which works in the mK regime. This was realized by keeping the microwave cavity and the electronics at room temperature, and inside a quartz finger tip only the sample was cooled down to mK (by means of a dilution refrigerator). Figure 3 shows the EPR of the Yb doublet ground state at 3 GHz at approximately 810 mK and 160 mK. From such a temperature-dependent measurement we were able to deduce T_K according to the above equations [12].

Nowadays this scenario has been picked up to study concentrated Kondo lattices in heavy fermion metals and is presented by J. Sichelschmidt at this conference [13]. Today Kondo resonances of single impurities of Co on metal surfaces are investigated by Scanning Tunneling Microscopy (STM). This technique is able to study the narrow Kondo resonance at the Fermi energy. The width of such a Kondo resonance is also determined by a characteristic Kondo temperature. Experiments in the future will show if the parameters determined from Kondo resonances in the electronic band structure do agree with the renormalization parameters determined from a logarithmic temperature dependence as shown above.

4. UHV-EPR/FMR IN NANOSTRUCTURED FERROMAGNETS

In the same way as EPR microwave cavities for 9, 4, and 1 GHz have been combined with the quartz finger tip and a dilution refrigerator, they can also be combined with an ultra high vacuum (UHV) chamber having the microwave setup in ambient laboratory air and only the sample under UHV conditions with surface science tools for sample preparation and characterization. This has been successfully used for EPR of paramagnetic molecules adsorbed in UHV on single crystal substrates with sub-monolayer coverage [14]. Usually, the sample size for EPR has a surface area of a few mm^2. This corresponds to 10^{14}–10^{15} atoms per monolayer (ML). Depending on the linewidth EPR has an ultimate sensitivity down to 10^{10}–10^{11} spins, that is to say it is sub-monolayer sensitive. One example is given in Fig. 4a. 1.6 ML Gd evaporated in UHV on a W(110) single crystal show a fairly good EPR signal at 318 K–far above T_C. The intensity increases close to T_C (Fig. 4b) but the signal is well detectable also in the paramagnetic regime [15]. In Fig. 5 the linewidth is plotted for Ni(111)/W(110). For a bulk Ni crystal the linewidth shows a narrow peak (only 7K broad) at $T_C = 632$ K. This divergence of the linewidth of Ni films decreases

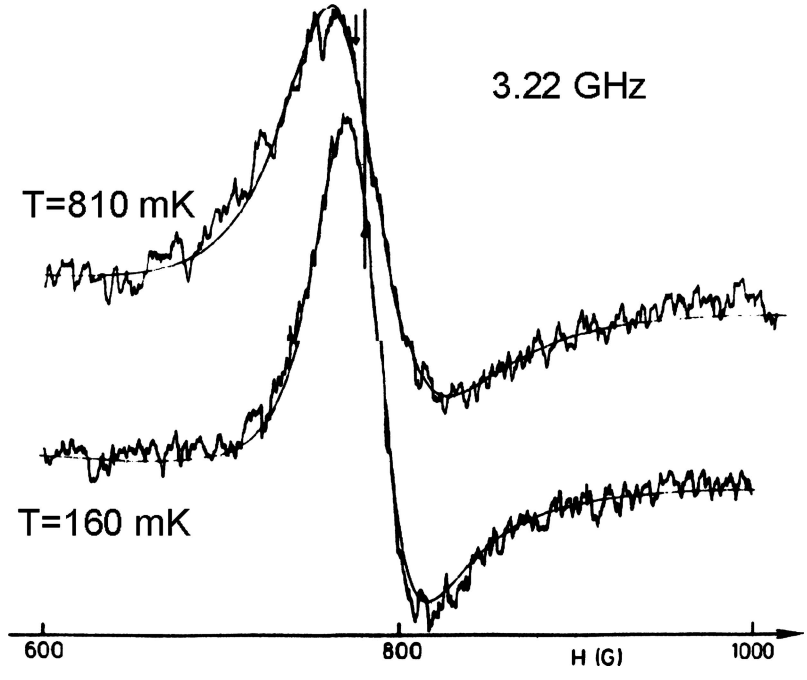

Fig. 3. EPR signal of 1200 ppm Yb in Au in the millikelvin regime with $T \geq T_K$ [12].

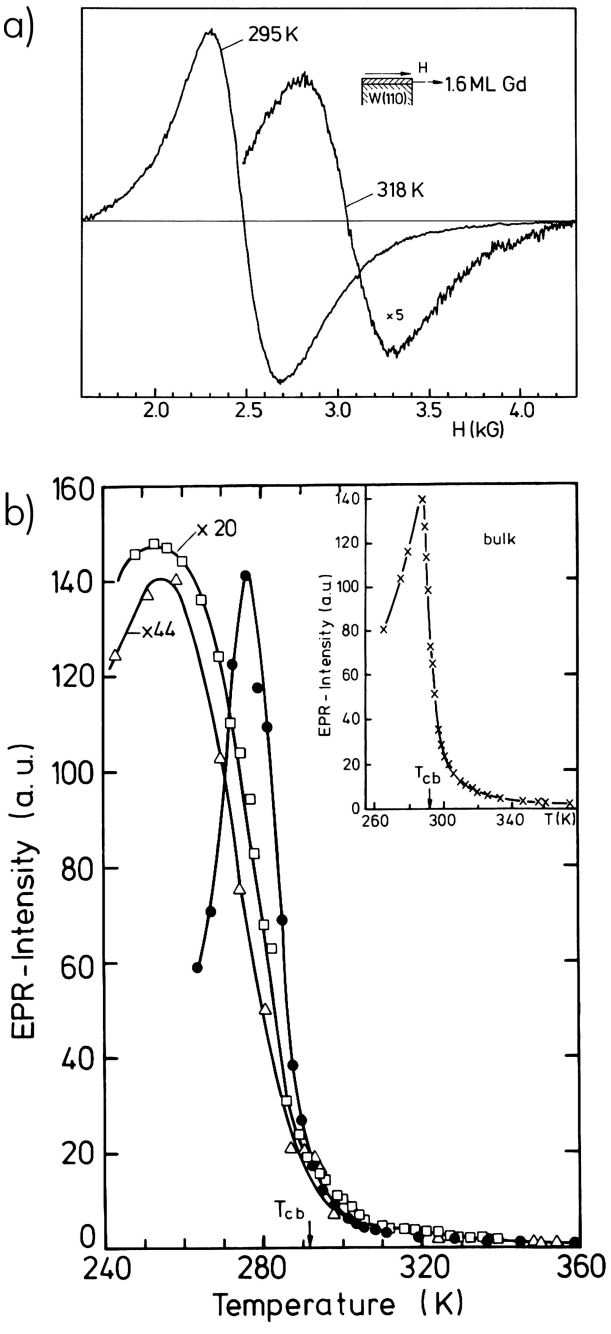

Fig. 4. *In situ* UHV-EPR of 1.6 ML Gd/W(110) at X-band. (a) In contrast to the Yb: Au resonance in Fig. 3 the Gd resonance is symmetric and shows no Dyson profile because the ultrathin film of Gd is "transparent" for themicrowave. (b) The EPR intensity above and below the T_C for various thicknesses: 0.8 ML (open triangles), 1.6 ML (*open squares*), and 80 Å (*full symbols*) [15].

to lower temperature for thinner films from 20 ML to 2 ML (Fig. 5). It corresponds to a reduction of T_C as a function of the thickness following the finite size scaling. Furthermore, the peak broadens the thinner the film, i.e., at the 3D → 2D phase transition the spin fluctuations are spread out over a larger temperature range. The detailed analysis of these data determining the critical exponent β and its crossover from 3D to 2D is discussed in [16]. There exist only a few examples in the EPR literature with such narrow divergence of the linewidth at the phase transition temperature. One is the EPR of paramagnetic Fe centers in $SrTiO_3$. K. A. Müller and coworkers show a very sharp divergence of the EPR linewidth at the structural phase transition at $T = 105$ K [17].

The resonance condition for FMR is given by the well-known Kittel formula

$$\frac{\omega^2}{\gamma_{||}^2} = H_0^2 + H_0\left(4\pi M - 2\frac{K_2}{M} + 4\frac{K_{4||}}{M}\right) + 2\frac{K_{4||}}{M}\left(4\pi M - 2\frac{K_2}{M} + 2\frac{K_{4||}}{M}\right). \quad (6)$$

In a dilute paramagnet the applied external Zeeman field is equal to the local field and the only unknown parameter is the g-factor. This is more complicated in the case of ferromagnets. Here, the local resonance field is a superposition of the external field H_0, the demagnetizing field 4 πM, and various contributions to the magnetic anisotropy energy (MAE) like K_2/M. These magnetic anisotropy contributions carry historically different names (magnetocrystalline anisotropy, magnetoelastic anisotropy, etc.) but they all have one common origin, namely the spin-orbit coupling. Only the anisotropy of the orbital magnetic moment μ_l, creates a magnetic anisotropy contribution in the free energy density [4,18]. Kittel also pointed out that the ratio of orbital to spin magnetic moment can be deduced from the measured g-value via $\mu_l/\mu_s = (g-2)/2$ [4,5]. However, a precise determination of the *g*-tensor is only possible if the anisotropy fields are determined very precisely—in most cases this is missing.

Magnetic multilayers are one of the most intensively studied nanostructured systems at present. The prototype system is a magnetic "trilayer," i.e., two ferromagnetic films separated by a nonmagnetic spacer, e.g., Ni/Cu/Co grown on a substrate crystal. Here, the UHV-FMR serves as a very powerful experimental tool. Each of the ferromagnetic films has its own anisotropy constant Eq. (6) and in addition

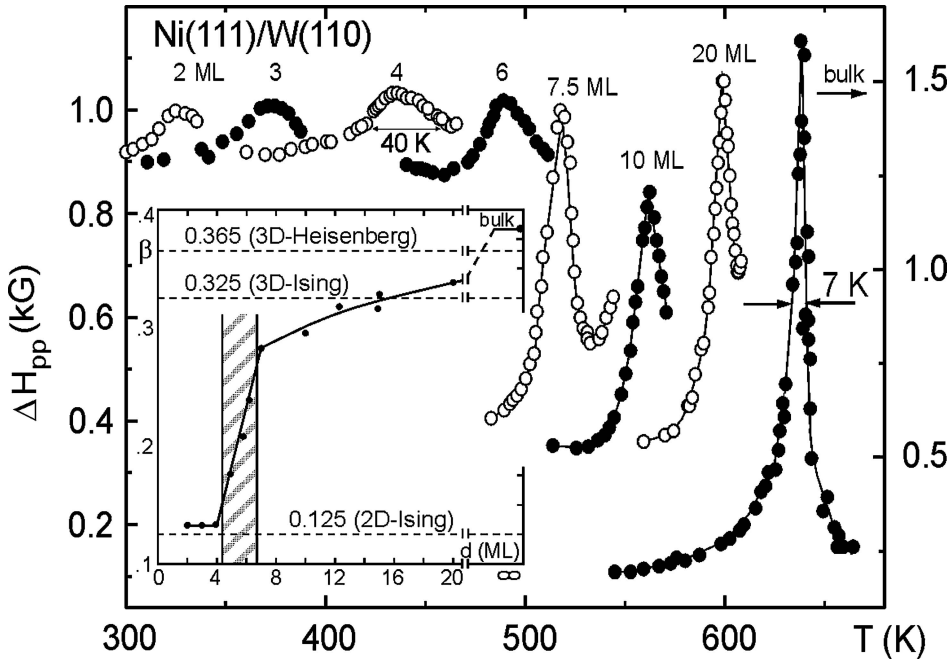

Fig. 5. The linewidth broadening at T_C for various thicknesses of Ni(111)/W(110). All films are prepared and measured *in situ* in UHV. For details see text and [17].

an IEC parameter J_{inter}. The equation of motion is given by the Landau–Lifshitz–Gilbert equation

$$\frac{1}{\gamma}\frac{\partial \vec{M}}{\partial t} = -(\vec{M} \times \vec{H}_{\text{eff}}) + \frac{G}{\gamma^2 M_S^2}\left(\vec{M} \times \frac{\partial \vec{M}}{\partial t}\right), \qquad (7)$$

where $\vec{M}$ is given by the sum $\vec{M} = \vec{M}_1 + \vec{M}_2$, and H_{eff} does not only include the anisotropy field of each individual film but also an additional exchange field parameterized by J_{inter}. Figure 6 gives one example: The upper part shows schematically that in analogy to coupled pendulums also a ferromagnetic trilayer has two eigenmodes an in-phase and an out-of-phase precession of the magnetization (the acoustic and optical mode). The middle part of Fig. 6 shows the simulations using Eq. (7). For $J_{\text{inter}} = 0$ (solid line) we get two resonance modes with equal intensity but different resonance positions depending on the individual anisotropy parameters. Switching on a finite IEC shifts the resonance position and transfers oscillator strength of the optical into the acoustic mode. Furthermore, the simulation shows nicely the different solutions for AFM and FM coupling having the optical mode at the higher and lower resonance field position, respectively. The lower part of Fig. 6 shows the

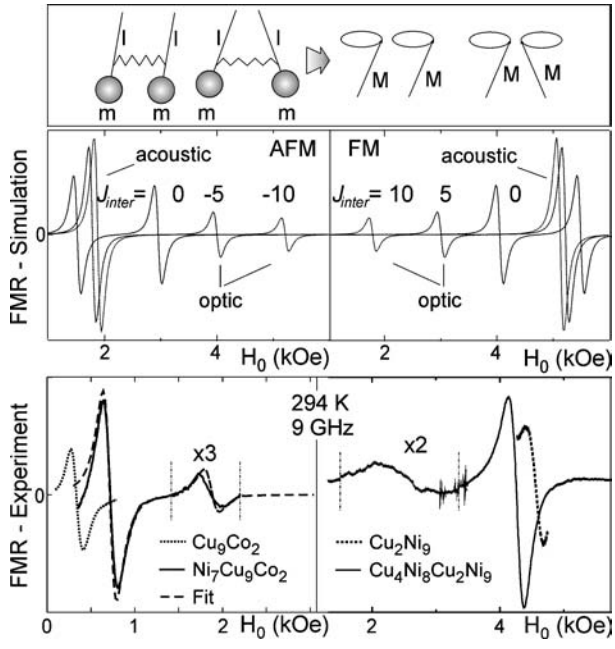

Fig. 6. FMR in a ferromagnetic trilayer. *Top*: schematic drawing of acoustic and optical modes. *Middle*: calculated FMR resonance using Eq. (7) for different IEC strength J_{inter} in arbitrary units. *Bottom*: corresponding experimental results for an AFM (*left*) and a FM (*right*) coupled trilayer [20].

corresponding experiment: on the left hand side, a $Ni_7/Cu_9/Co_2$ AFM coupled trilayer; on the right hand side $Ni_8/Cu_2/Ni_9$ FM coupled. In a detailed sequence of experiments varying the IEC (Cu thickness) or the temperature (changing $J_{inter}(T)$) the FMR supplies a complete set of detailed information about the temperature dependence of the coupling [19] and the oscillatory behavior of the IEC. For a detailed review see [20]. The *in situ* UHV-FMR also offers the possibility to perform a "step-by-step experiment," i.e., measuring first a single FM film and then studying the influence of the *in situ* prepared trilayer. The lower part of Fig. 6 shows the dotted lines of a single Co and a single Ni film, respectively and its modification after preparation of the full trilayer. In the same sense also the influence of surface effects can be investigated. How does the magnetic anisotropy of a single Ni film change, if the Ni surface faces (i) vacuum, (ii) is capped by a nonmagnetic Cu film or (iii) oxygen is adsorbed on the surface [21]?

5. FMR LINE WIDTH AND "SPIN-PUMPING"

So far we have discussed only the resonance field H_{res} of an FMR experiment and the detailed information one might obtain (angular dependence, temperature dependence, FM and AFM coupling). This covers almost 95% of the FMR literature. However, the magnetic resonance provides us much richer information. In this section we will focus on the linewidth. The standard form to discuss linewidth and damping, respectively, in the FMR is the so-called Gilbert damping, the second term in Eq. (7). In the following we will show that this might be an oversimplified ansatz. Almost everybody working on fast switching or reversal dynamics in magnetic nanostructures uses Eq. (7) with the Gilbert damping. The derivative with respect to time $\partial M/\partial t$ implies that the damping is proportional to ω, a friction-like damping proportional to the velocity. Such a viscosity-like damping is a dissipative mechanism in which the energy stored in the motion of the magnetization relaxes to the thermal bath heating the sample. In the language of EPR this corresponds to the longitudinal T_1 relaxation. However, we know that there is also a transverse relaxation mechanism T_2 for the M_x and M_y components. (This energy might also relax at the end to the thermal bath, but for the moment it is still stored in the magnetic reservoir.) In a ferromagnet this translates into magnon–magnon scattering. The uniform motion of magnetization might scatter into other magnons with finite k-vectors. For such a mechanism it is by no means obvious that this should be proportional to ω. The upper part of Fig. 7 shows this schematically. An experimental linewidth of ΔH may have some ω-proportional damping mechanism (dashed line). It may also have some inhomogeneous residual linewidth, but it may also have a magnon–magnon scattering contribution with a completely different ω-dependence (dotted line) as predicted by R. Arias *et al.* [22]. Due to the experimental difficulty to work with microwaves of different frequency, most of the experimental results restrict themselves to 10–35 GHz. It is clear that for such a narrow frequency range in a first approximation of a Taylor expansion one might be attempted to deduce a linear frequency dependence (as indicated in Fig. 7). Recently, FMR experiments on Fe/V multilayers have been performed over a large range of frequency [23]. To verify such a curved frequency dependence of $\Delta H(\omega)$ it is equally important to measure at very low frequency down to 1 GHz. The full squares in the experimental results (lower

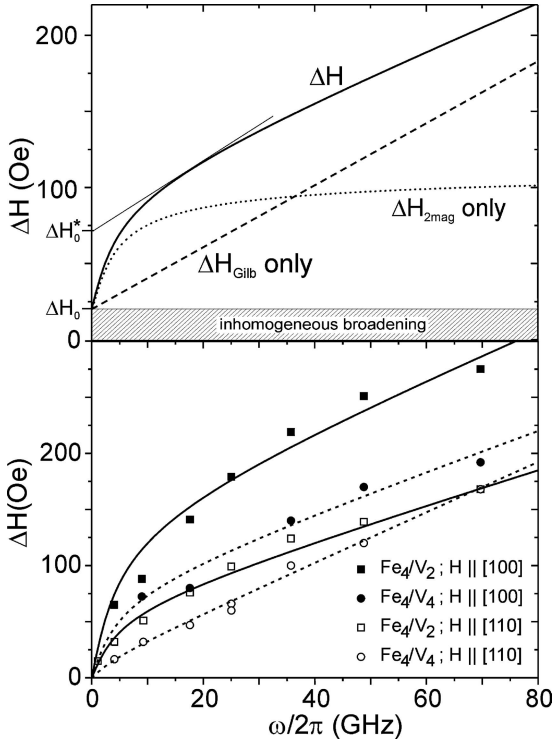

Fig. 7. FMR linewidth ΔH as a function of the microwave frequency. Schematic drawing (*top*) and corresponding experiments (*bottom*). Note that the strength of the two magnon contribution depends on the crystallographic orientation (full *vs.* open symbols).

part of Fig. 7) verify clearly the "non-Gilbert-type" spin wave damping. These magnon–magnon scattering effects seem to be more important in magnetic nanostructures than in bulk material, if geometric structures (at interfaces, surfaces) of nanometers are in the same order of magnitude as the wavelength of the magnons.

The dynamics of the ferromagnetic magnetization at an interface to nonmagnetic metals in nanostructures have been addressed by A. Janossy and coworkers [24]. They could show that the uniform precession of the ferromagnetic magnetization couples via the s-d-exchange to the conduction electrons of a nonmagnetic metal like Au. In other words, the precession of M "pumps" the conduction band of Au. This was used to detect the conduction electron spin resonance (CESR); the ferromagnet was used to enhance the oscillatory microwave field. This mechanism has recently been reactivated for magnetic trilayers (see Fig. 6) in which the optical and acoustic modes of FM1 and FM2 show a dramatic narrowing of the FMR linewidth if both resonance fields coincide as a function of the angle. This has been shown for Au spacers of approximately 40 ML [25] and for ultrathin Cu spacer [26].

6. CONCLUSION

The combination of EPR with UHV and surface science technology makes magnetic resonance a very powerful technique for today's enormous effort in the spectroscopy of nanostructures. Nanoscaled structures must be prepared under UHV conditions and EPR can measure them *in situ*. The technique allows to measure the paramagnetic as well as the FM ordered state. The temperature and angular dependence of the resonance field are converted in proper energy units (eV/spin), this is hardly to achieve by other techniques. Absolute numbers of IEC and MAE bridge to the *ab initio* calculations and serve for a better understanding of magnetism on an atomic level.

ACKNOWLEDGMENTS

We acknowledge C. Sorg and E. Kosubek for the preparation of this manuscript. Parts of this work were supported by the DFG(Sfb 290).

REFERENCES

1. E. K. Zavoisky, Doctoral thesis, Moscow (1944); *J. Phys. USSR* **9,** 245 (1945).
2. http://kfti.knc.ru/eng/zavoisky/awholders.html
3. S. A. Al'tshuler, Proceedings of the XIVth Colloque Ampère, 588 (1966).
4. A. Abragam and B. Bleaney, *Electron Paramagnetic Resonance of Transition Ions* (Clarendon Press, Oxford, 1970).
5. Ch. Kittel, *Phys. Rev.* **73,** 155 (1948); Ch. Kittel, *Phys. Rev.* **76,** 743 (1949).
6. S. A. Al'tshuler, I. A. Garifullin, and E. G. Kharakhash'yan, *Sov. Phys. Sol. State* **14,** 213 (1972).
7. A. A. Abrikosov and L. P. Gor'kov, *J. Exptl. Theoret. Phys. (U.S.S.R)* **39,** 1781 (1960).
8. N. E. Alekseevskii, I. A. Garifullin, B. I. Kochelaev, and E. G. Kharakhash'yan, *ZhETF Pis. Red.* **18,** 323 (1973).
9. C. Rettori, D. Davidov, P. Chaikin, and R. Orbach, *Phys. Rev. Lett.* **30,** 437, (1973).
10. U. Engel, K. Baberschke, G. Koopmann, S. Hüfner, and M. Wilhelm, *Solid State Commun.* **12,** 977 (1973).
11. K. Baberschke, K. D. Bures, and S. E. Barnes, *Phys. Rev. Lett.* **53,** 98 (1984).
12. K. Baberschke and E. Tsang, *Phys. Rev. Lett.* **45,** 1512 (1980).
13. J. Sichelschmidt, *et al.*, this conference (2004).
14. M. Zomack and K. Baberschke, *Surf. Sci.* **178,** 618 (1986).
15. M. Farle and K. Baberschke, *Phys. Rev. Lett.* **58,** 511 (1987).
16. Yi Li and K. Baberschke, *Phys. Rev. Lett.* **68,** 1208 (1992).
17. Th. von Waldkirch, K. A. Müller, and W. Berlinger, *Phys. Rev. B* **7,** 1052 (1973).
18. K. Baberschke, *Appl. Phys. A* **62,** 417 (1996).
19. J. Lindner, *et al.*, *Phys. Rev. Lett.* **88,** 167206 (2002).
20. J. Lindner and K. Baberschke, *J. Phys.: Cond. Matt.* **15,** R193 (2003).
21. Jisang Hong, *et al.*, *Phys. Rev. Lett.* **92,** 147202 (2004).
22. R. Arias and D. L. Mills, *Phys. Rev. B* **60,** 7395 (1999).
23. J. Lindner, *et al.*, *Phys. Rev. B* **68,** 060102 (R) (2003).
24. R. H. Silsbee, A. Janossy, and P. Monod, *Phys. Rev. B* **19,** 4382 (1979).
25. B. Heinrich, *et al.*, *Phys. Rev. Lett.* **90,** 187601 (2003), and B. Heinrich at this conference.
26. K. Lenz, *et al.*, *Phys. Rev. B* **69,** 144422 (2004).